Optimal ion channel clustering for intracellular calcium signaling

J. W. Shuai* and P. Jung

Department of Physics and Astronomy and Quantitative Biology Institute, Ohio University, Athens, OH 45701

Edited by John Ross, Stanford University, Stanford, CA, and approved November 21, 2002 (received for review October 7, 2002)

Ion channels and receptors in the cell membranes and internal membranes are often distributed in discrete clusters. One particularly well-studied example is the distribution of inositol 1,4,5-triphosphate receptors in the plasma membrane that controls the flux of Ca^{2+} from the endoplasmic reticulum into the cytosol. By using mathematical modeling, we show that channel clustering can enhance the cell's Ca^{2+} signaling capability. Furthermore, we predict optimal signaling cellular capability at cluster sizes and distances that agree with experimentally found values in *Xenopus* oocyte.

channel dynamics | Markov process | noise

Receptors and ion channels play an important role in cellular homeostasis. They regulate electric membrane potentials and cell volume and turn on and off signaling cascades within the cell. Highly resolved fluorescent imaging and antibody labeling technology have revealed that the channel and receptor proteins are frequently not uniformly distributed over the membrane but rather form small clusters sometimes only on the nanometer scale (for a review see ref. 1). One possible mechanism that leads to clustering is based on the formation of microdomains of the lipid bilayer of the membrane. These microdomains, the so-called rafts (2), are more likely to bind specific proteins and form a, possibly moving, platform for protein trafficking, or signal relay stations for intracellular signaling. Other proposed mechanisms for clustering involve the cytoskeleton (3). Here, microtubules in the membrane undercoat anchor channels that otherwise would perform free motion through the cell membrane. As a result, μm^2-sized clusters of ion channels form on the axon of e.g., rat retinal ganglion cell. In recent work by Clay and Kuzirian (4–6) it has been discovered that potassium channels in the squid giant axon are clustered. Evidence has been presented that vesicles containing potassium channels are contacting the cluster sites and facilitate channel turnover.

Clustering of chemotactic receptors on *Escherichia coli* has been shown to constrain sensitivity of signaling in response to receptor binding (7). Binding of the chemotactic receptor inactivates a downstream intracellular signaling pathway. If there is cooperativity between neighboring receptors, in the sense that an activated receptor in turn activates receptors in its neighborhood, it is clear that this cooperativity will enhance the response by increasing the change in number of activated receptors. If the numbers of receptors is limited, however, increasing spatial range of cooperation between the receptors (i.e., cluster sizes) increases the response to a small number of binding agonist but does not leave room for differential response to stimuli of different intensity. It has been proposed that distributions of receptors in clusters of variable sizes optimize the response to small stimuli and the sensitivity to signal amplitudes (7).

We propose a different role for the clustering of receptors and ion channels in the membrane. We do not attempt to answer the question of what the molecular mechanism for clustering may be, but we rather point out some consequences of channel clustering with respect to signaling capability. As a working example we consider intracellular Ca^{2+} signaling because experimental data on clustering are available as well as generally accepted mathematical models (8–10). Many important cellular functions are regulated by intracellular and intercellular Ca^{2+} signals. They are involved, e.g., in the stimulus-induced contraction in smooth muscle cells (11), in the hormone-induced glucose production in liver cells (12), and for the early response to injury of brain tissue (13) and corneal epithelia (14). Recent new insights into the biophysical mechanism of intracellular Ca^{2+} release have revealed that the actual release sites are discrete and as small as $\approx$100–200 nm comprising only 20–50 release channels (15–17). The clustering of these channels is well documented in various cell types and may be a universal feature of the Ca^{2+} release mechanism.

In the next section we will give a detailed account of the model. Then we will discuss the prediction of our model with respect to Ca^{2+} signaling as a response to agonist binding and subsequent activation of the G protein-coupled signaling pathway. We will show that signaling capability is modified with the discrete distribution of the Ca^{2+} release channels. We will determine an optimal configuration of release channels and compare these optimal values to experimental data on clustering.

Model for Intracellular Ca^{2+} Response

Ca^{2+} is stored in the endoplasmic reticulum (ER) because it is toxic for the cell if the cell is exposed for a sufficient amount of time to large concentrations. Ca^{2+} can enter the cytosol via channels in the plasma membrane of the ER. The flux through these channels is determined by the concentration of Ca^{2+} in the cell and by that of the messenger inositol 1,4,5-triphosphate (IP_3). According to the detailed DeYoung–Keizer model (18) the IP_3 receptor (IP_3R) channels consist of three subunits, each of which has to be in its open state for the channel to be open. Each subunit has three binding sites: one for IP_3 and two for Ca^{2+}. The first Ca^{2+} binding site activates the subunit whereas the second binding site inactivates the subunit. Because there is a vast difference in the time scale of these three binding processes, one can replace the fast IP_3 binding and Ca^{2+} activation by their average values and only consider the inactivation process dynamically. Such an elimination process results in a two-variable model for the receptor dynamics (19). The cell is modeled as a 2D sheet with two domains: the cytosol and the ER. The sheet is assumed to be thin so that the Ca^{2+} concentration ($[Ca^{2+}]$) in the cytosol and the ER is homogenous across it. The two domains interact via the release of Ca^{2+} from ER into the cytosol through discretely distributed receptor channels and subsequent diffusion and reuptake by the ER. The smallness of the release clusters requires stochastic modeling of their conductance. All intracellular Ca^{2+} buffers are assumed to be fast so that their presence can be modeled by an effective diffusion coefficient (values have been experimentally determined). The IP_3Rs are distributed in clusters positioned on a regular grid. The total number of IP_3Rs is considered fixed while they can be

This paper was submitted directly (Track II) to the PNAS office.

Abbreviations: ER, endoplasmic reticulum; IP_3, inositol 1,4,5-triphosphate; IP_3R, IP_3 receptor; $[Ca^{2+}]$, Ca^{2+} concentration.

*To whom correspondence should be addressed. E-mail: shuai@helios.phy.ohiou.edu.

 www.pnas.org/cgi/doi/10.1073/pnas.0236032100

distributed differently, ranging from numerous small clusters (with possibly only one channel) at a small distance to few large clusters at larger distances. The equation for the intracellular $[Ca^{2+}]$ is given by

$$\frac{d[Ca^{2+}](x,y)}{dt} = D\nabla^2[Ca^{2+}](x,y) + f(x,y)J_{Channel} - J_{Pump} + J_{Leak}, \quad [1]$$

where $[Ca^{2+}]$ can diffuse in the cytosol with diffusion constant D. In the presence of fast buffers, the diffusion constant has to be interpreted as effective diffusion constant. The form function $f(x, y)$ is unity at a cluster of $[Ca^{2+}]$ release channels and zero elsewhere. There are three fluxes of $[Ca^{2+}]$ between the cytosol and the ER. The channel flux $J_{channel}$ describes the $[Ca^{2+}]$ flux through the release channels and is localized at the cluster sites, the flux J_{Pump} describes the Ca^{2+} reuptake through sarco(endo)-plasmic reticulum Ca^{2+} ATPase pumps, and J_{Leak} describes leak flux. The pumps and leaks are assumed homogeneously distributed over the plasma membrane of the ER and their fluxes are given by

$$J_{Pump} = v_P \frac{[Ca^{2+}]^2}{k^2 + [Ca^{2+}]^2} \quad [2]$$

$$J_{Leak} = v_L([Ca^{2+}]_{ER} - [Ca^{2+}]), \quad [3]$$

where $[Ca^{2+}]_{ER}$ denotes the $[Ca^{2+}]$ in the ER.

To complete the model, we have to specify the channel flux. We use the stochastic version (20) of the Li–Rinzel model (16), which is a reduction of the more detailed stochastic DeYoung–Keizer model (18) but is still accurate for processes on the time scale of seconds (21). The channels are concentrated in clusters of <0.5 μm diameter, which is much smaller than the diffusion length of Ca^{2+} with a physiologic diffusion constant of $D \approx 20$ $\mu m^2/s$. This small size of a cluster allows us to assume that the Ca^{2+} is constant within the cluster (see also ref. 17). This in turn allows us to model the Ca^{2+} flux from the ER into the cytosol as a point source with a weight factor that describes the strengths (size) of the source. That results in a Ca^{2+} flux through cluster i, given by

$$J^{(i)}_{Channel} = v_C m_\infty^3 n_\infty^3 N^{(i)}_{open}([Ca^{2+}]_{ER} - [Ca^{2+}]), \quad [4]$$

where v_C contains the ratio of channel size and grid size and

$$m_\infty = \frac{[IP_3]}{[IP_3] + d_3}$$
$$n_\infty = \frac{[Ca^{2+}]}{[Ca^{2+}] + d_5}, \quad [5]$$

where the number of open channels of cluster i N^i_{open} is determined by a Markov process describing the state of each channel. Each cluster has N IP_3R channels. The three subunits of the IP_3R result in three gates in the reduced model, with opening and closing rates α_h and β_h, respectively, given by

$$\alpha_h = a d_2 \frac{[IP_3] + d_1}{[IP_3] + d_3}$$
$$\beta_h = a[Ca^{2+}]. \quad [6]$$

This approach is standard and we refer the reader to the literature for details (e.g., ref. 22).

The size of the cell simulated is 60 μm $\times$ 60 μm. In the simulations presented here, the total number of channels in the entire cell was fixed at 14,400 channels. The computer cell thus has the form of mosaic of active and passive (still nonlinear) patches. Of critical importance is the diffusion constant of Ca^{2+} in the cytosol. The effective diffusion coefficient of Ca^{2+} in the cytosol reported in the literature ranges from 20 to 30 $\mu m^2/s$ (23). In our simulations we will cover this interval of diffusion coefficients. The parameter values in the model are: $v_C = 0.6\ s^{-1}$, $v_P = 0.5\ s^{-1}$, $v_L = 0.001$ μM/s, $[Ca^{2+}]_{ER} = 15.0$ μM, $k = 0.1$ μM, $a = 0.2$ $\mu M^{-1}\cdot s^{-1}$, $d_1 = 0.13$ μM, $d_2 = 1.05$ μM, $d_3 = 0.94$ μM, $d_4 = 0.13$ μM, and $d_5 = 0.08$ μM. These parameters are slightly modified from the original Li–Rinzel model (19). As a result of these simulations we determine the spatially averaged (over the entire cell) Ca^{2+} and Ca^{2+} recordings at selected sites.

Results and Discussion

We start with single channels distributed homogeneously at a distance of $L = 0.5$ μm over a cell, i.e., in 120×120 clusters of single channels ($N = 1$) at a physiologic diffusion coefficient of $D = 20$ $\mu m^2/s$ and $[IP_3] = 0.21$ μM. The Ca^{2+} traces shown in Fig. 1 *A2* and *A3* are obtained from two neighbored cluster sites. They are correlated with small amplitudes and no temporal coherence (periodicity). The cell-averaged Ca^{2+} signal (Fig. 1*A1*) does not exhibit spikes that could be interpreted as a signal in response to the stimulation by IP_3. For smaller diffusion coefficients D, the channels are less synchronized but also lead to a spike-free cell-averaged Ca^{2+} response of the entire cell (not shown).

In the next step we increase the distance L of the clusters of the IP_3Rs but increase their sizes (i.e., numbers of channels N) so that the total number of channels remains 14,400. Traces of Ca^{2+} taken at two neighbored cluster sites and the cell-averaged $[Ca^{2+}]$ are shown for $D = 20$ $\mu m^2/s$ and $[IP_3] = 0.21$ μM in Fig. 1 *B2* and *B3* at a cluster distance of $L = 3$ μm. The Ca^{2+} traces at the neighbored active sites are now almost periodic with some stochasticity in the amplitude, but well phase synchronized. Most importantly, the cell-averaged Ca^{2+} response (Fig. 1*B1*) is almost periodic with some stochasticity in the amplitude that is orders of magnitude larger than in the previously discussed case where the cluster distance was only 0.5 μm. Such a coherent behavior enables the distributed Ca^{2+} decoder calmodulin to interpret the signal generated by the IP_3 stimulus.

Increasing the distance between the clusters further to $L = 5$ μm with a cluster size of $N = 100$ channels results again in stochastic, desynchronized Ca^{2+} signals at the two neighbored cluster sites (Fig. 1 *C2* and *C3*). The cell-averaged Ca^{2+} signal (Fig. 1*C1*) is temporally incoherent with a small amplitude. Thus, similar to the homogeneous clustering in Fig. 1, the cell cannot produce a global Ca^{2+} signal on stimulation with IP_3. It is important to keep in mind that the values for the intracellular diffusion coefficient D of Ca^{2+} and the concentration of $[IP_3]$, i.e., the amplitude of stimulation by agonist binding, are the same in Fig. 1.

To quantify the signaling capability of the entire cell we record the minimum and maximum of the computed cell-averaged $[Ca^{2+}]$ as a function of the cluster distance. Such diagrams are shown for $[IP_3] = 0.21$ μM and various values of D in Fig. 2. Large gaps between minimum and maximum amplitude go along with spatiotemporal coherence as shown in Fig. 3 (discussion below). For small and large cluster distances, minimum and maximum amplitudes are very close (see Fig. 2), i.e., the cell is not capable of signaling on weak IP_3 stimulation. In between, we find intervals of cluster distances at which the cell is capable of generating large amplitude and coherent Ca^{2+} signals that may be decoded in the cell to trigger processes downstream.

At the physiologic value of the (buffered) Ca^{2+} diffusion constant of 20 $\mu m^2/s$, the regime where the cell signals optimally ranges from 2 to 3 μm at $[IP_3] = 0.21$ μM, which is remarkably close to average cluster distances measured in *Xenopus* oocyte (15, 16). Furthermore, the corresponding

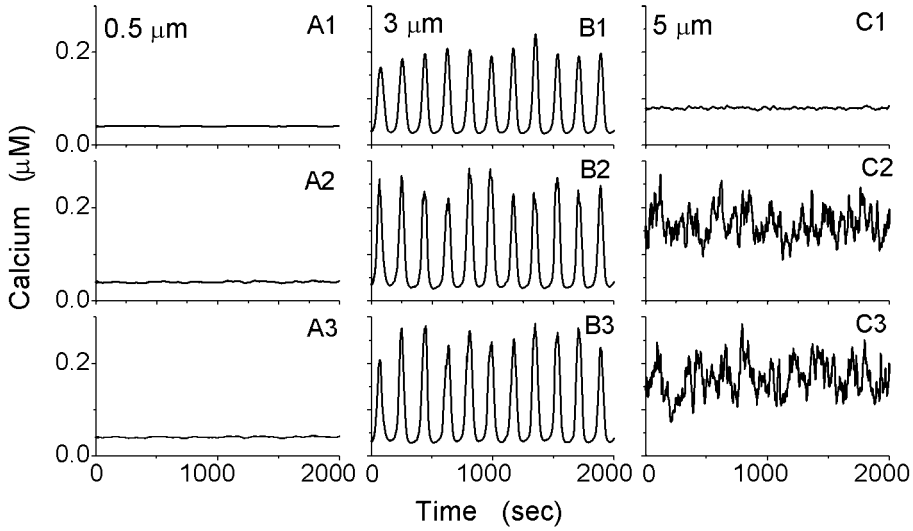

Fig. 1. $[Ca^{2+}]$ at two neighbored active sites 0.5 μm apart (*A2* and *A3*), 3 μm apart (*B2* and *B3*), and 5 μm apart (*C2* and *C3*) and the corresponding cell-averaged $[Ca^{2+}]$ (*A1*, *B1*, and *C1*). The other parameters are $D = 20\ \mu m^2/s$ and $[IP_3] = 0.21\ \mu M$.

number of channels per cluster ranges from 16 to 36, which is also consistent with the prediction obtained with independent methods in ref. 17.

Some spontaneous Ca^{2+} waves are shown in Fig. 3. The top row in Fig. 3 shows a sequence of snapshots for $[IP_3] = 0.21\ \mu M$ and $D = 20\ \mu m^2/s$ at a cluster distance of 1.5 μm. There is no significant Ca^{2+} signal generated on the stimulation with IP_3. For cluster distances between 2.0 and 3.0 μm there is a clearly visible Ca^{2+} response that is repetitive. At a cluster distance of 2 μm (second row from the top in Fig. 3), the Ca^{2+} signal consists of a repetitive abortive wave. It is initiated in the lower left corner, spreads out, but then retreats again. Such waves have been observed in *Xenopus* oocyte (15) and theoretically predicted in ref. 10. At cluster distances of 2.5 and 3.0 μm we observe global oscillations generated by Ca^{2+} waves initiated at multiple initiation sites (third and fourth rows from the top in Fig. 3). The average oscillation frequency for the cell-averaged Ca^{2+} signals is 0.02 and 0.03 Hz for these two waves, respectively. These frequencies are consistent, but somewhat smaller than the oscillation frequency at the onset of deterministic oscillations at

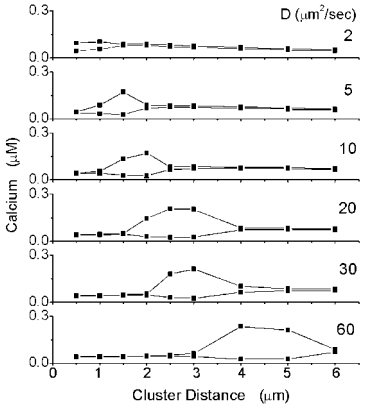

Fig. 2. The minimum and maximum amplitudes of the cell-averaged Ca^{2+} are shown as a function of the cluster distance. In a small interval of cluster distances, there is a large gap between the minimum and the maximum amplitude, indicating a signal of large amplitude. In the same intervals, the cell-averaged Ca^{2+} signals are also temporally coherent and the clusters are phase-synchronized.

$[IP_3] \approx 0.24\ \mu M$. At a cluster distance of 4 μm the activity consists of local Ca^{2+} puffs with little cross-correlation.

Consistent with the observations above, the cluster–cluster correlations defined by the correlation time τ_c of the cluster–cluster correlation function

$$\tau_c = \int_0^\infty d\tau \left[\frac{\langle \tilde{x}_1(t)\tilde{x}_2(t+\tau)\rangle}{(\langle \tilde{x}_1^2\rangle\langle \tilde{x}_2^2\rangle)^{1/2}} \right]^2, \quad \tilde{x} = x - \langle x\rangle, \qquad [7]$$

exhibits *at* $D = 20\ \mu m/s^2$ a maximum at a cluster distance of $\approx 3\ \mu$m (see Fig. 4).

To understand the observed phenomenon of optimal clustering, we have to go one step back and reconsider the Ca^{2+} cluster release dynamics in the absence of diffusion and interaction with other clusters. For a large number of channels this release dynamics is described by the deterministic model

$$\frac{d[Ca^{2+}]}{dt} = J_{Channel} - J_{Pump} + J_{Leak}, \qquad [8]$$

with

$$J_{Channel} = v_C m_\infty^3 n_\infty^3 h^3([Ca^{2+}]_{ER} - [Ca^{2+}])$$
$$\frac{dh}{dt} = \alpha_h(1-h) - \beta_h h, \qquad [9]$$

where h is the fraction of occupied inhibitive Ca^{2+} binding sites of the IP_3R (19). The $[Ca^{2+}]$ resulting from Eqs. **8** and **9** as a function of the second messenger $[IP_3]$ is shown in Fig. 5. Below a concentration of IP_3 of 0.24 μM the equations predict a stable stationary concentration of Ca^{2+}. Beyond it, the model predicts Ca^{2+} oscillations. Small clusters of IP_3Rs cannot be described by this deterministic model; channel fluctuations require the use of stochastic models. A stochastic version of the Li–Rinzel model has been described in detail (20, 21, 24). Important in this context is the finding that the Ca^{2+} signals of a cluster in response to deterministically subthreshold IP_3 concentrations (i.e., weak stimulation) exhibit a small degree of periodicity if the clusters are within a range of optimal sizes (24). The effect is due to conductance fluctuations that assist in occasionally shifting the cluster above the oscillations

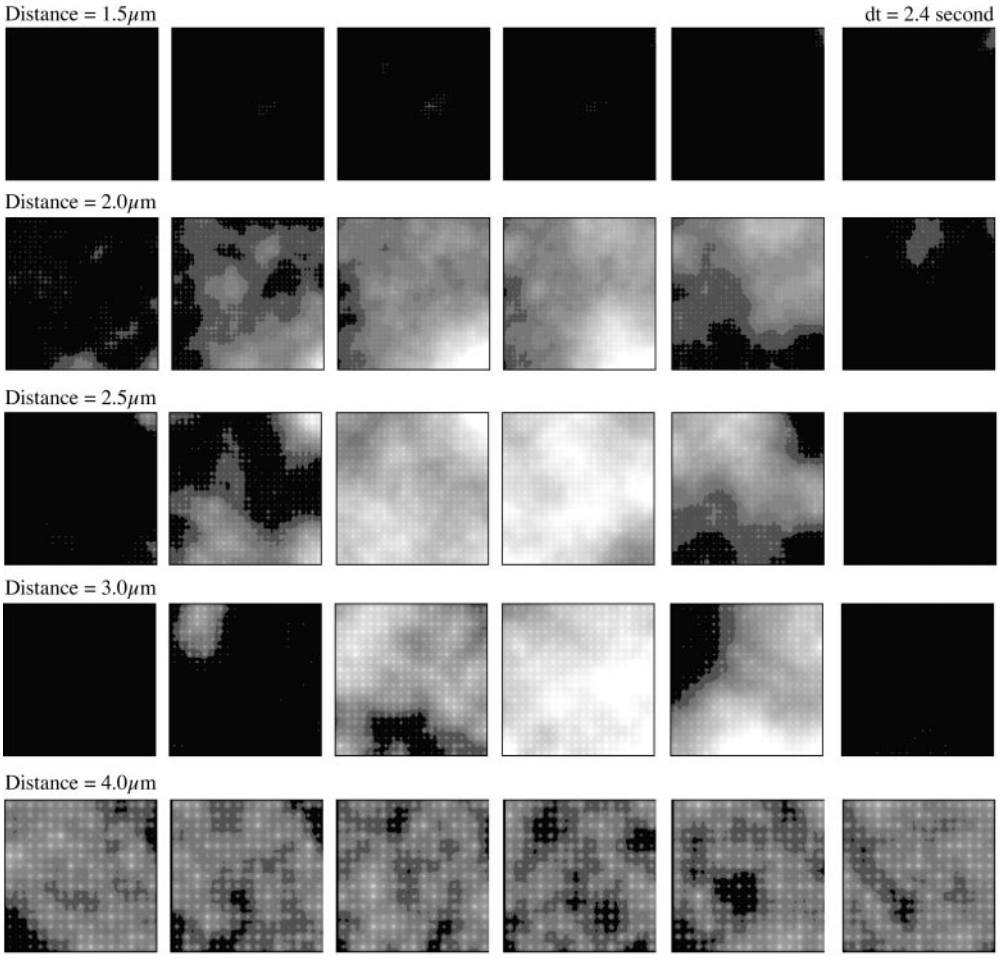

Fig. 3. Snapshots of the $[Ca^{2+}]$ are shown at five different cluster distances at $[IP_3] = 0.21\ \mu M$ and $D = 20\ \mu m^2/s$. Each snapshot has a size of 60 μm × 60 μm. The gray scales from black to white represent $[Ca^{2+}]$ from 0.05 to 0.25 μM.

threshold of 0.24 μM. This effect, however, is very subtle and may not be detectable by the cell. A related effect has been described in refs. 25 and 26. In those articles it has been shown that a single cluster of neuronal Na^+ and K^+ channels responds to a weak, subthreshold electric AC stimulation best at a finite cluster size.

In the spatially extended model for the entire cell, small cluster distances correspond to small clusters (1−10 channels) that release Ca^{2+} stochastically with little coherence. The thermal noise-induced subunit and channel openings dominate the Ca^{2+} release of the cluster. For small diffusion coefficients D the cell responds with uncorrelated events at the discrete release sites. For large diffusion coefficients D (like the physiological value of 20 $\mu m^2/s$ with a diffusion length of tens of micrometers), the clusters correlate and behave more like one large cluster with all channels of the cell, where open-closed fluctuations are exceed-

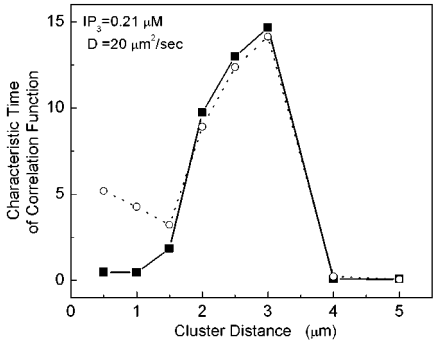

Fig. 4. The cross-correlation time (see Eq. **7**) of two nearby clusters at the center of the cell model (dashed line) and between the cell-averaged Ca^{2+} signal and the Ca^{2+} signal of the center cluster (solid line) for $[IP_3] = 0.21\ \mu M$ and $D = 20\ \mu m^2/s$ is shown as a function of the cluster distance.

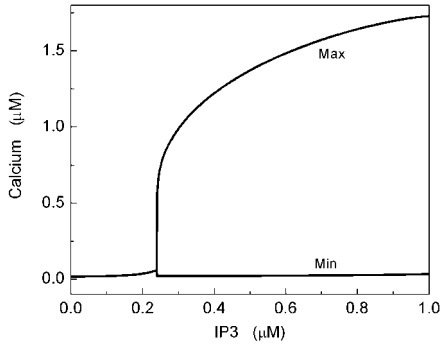

Fig. 5. The bifurcation diagram of the deterministic Li–Rinzel model is shown for our set of parameters. For concentrations of IP_3 of $<0.24\ \mu M$, the $[Ca^{2+}]$ approaches a fixed point. Above that concentration, the $[Ca^{2+}]$ oscillates and the minimum and maximum amplitudes are shown.

ingly unlikely, thus resulting in very weak Ca^{2+} signals (Fig. 1*A*). Increasing the distance between the clusters (thereby increasing the cluster size) reduces their tight coupling, thus allowing for spontaneous Ca^{2+} events. Yet, the coupling is still large enough that cross-synchronization between clusters enhances the temporal coherence. This coupling leads to the onset of spatially and temporally coherent oscillations (see also ref. 27) that decode the IP_3 signal. At an IP_3 concentration of 0.21 μM (Fig. 1*B*) this optimal clustering is reached when the clusters comprise 16–64 channels. Further increasing the distance between the clusters desynchronizes the clusters while each individual cluster still exhibits large-amplitude stochastic Ca^{2+} release. Averaging these desynchronized cluster responses to obtain the decidable cell-averaged Ca^{2+} response one finds the small signal in Fig. 1*C*.

If the concentration of IP_3 increases beyond the critical concentration of 0.24 μM, the effect of optimal clustering disappears. The best cell signal is achieved when the channels are homogeneously distributed. In Fig. 6, we show the minima and maxima of the Ca^{2+} signals as a function of the cluster distance for various Ca^{2+} diffusion constants D at $[IP_3] = 0.25$ μM. Increasing cluster size and thus cluster distance reduces the cell signal. At $D = 20$ $\mu m^2/s$ the cellular Ca^{2+} signal vanishes at distances of $L = 4$ μm and larger. For distances such as 2 μm or less, however, the clustering does not degrade the cellular signal significantly so that the cell can still respond to large signals with large amounts of IP_3 with a coherent cellular Ca^{2+} signal.

In conclusion, we have reported that channel clustering can dramatically enhance the cell's capability of creating a large Ca^{2+} response to weak stimulation. The theory predicts an optimal clustered distribution consistent with experimental data from *Xenopus* oocyte. In the model the effects of slow Ca^{2+} buffers are neglected. In the real cell, the clusters of Ca^{2+} release channels are not arranged on a regular grid and do not have the same channel numbers as in our model. We furthermore assumed that

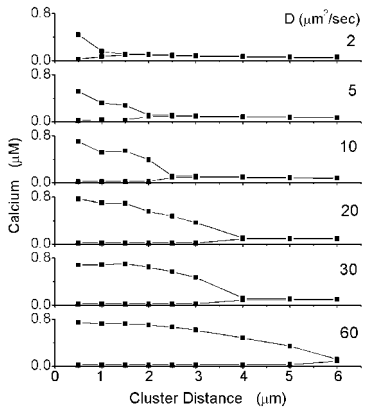

Fig. 6. The minimum and maximum amplitudes of the cell-averaged Ca^{2+} signals are shown as a function of the cluster distance at $[IP_3] = 0.25$ μM. The Ca^2 signal present at small cluster distances disappears when the clusters become too far apart to synchronize.

the $[Ca^{2+}]$ in the ER is homogeneous and time independent. For the parameters used here, the $[Ca^{2+}]$ in the ER is large in comparison to the intracellular $[Ca^{2+}]$ and the gradients are small so that the overall effect of Ca^{2+} diffusion in the ER is small. Future research will have to consider more details. We believe that similar consequences of ion channel clusters can be found in many other cell types and may play an important role in signal transduction in general and for electric signals in e.g., neurons.

This material is based on work supported by National Science Foundation Grant IBN-0078055.

1. Damjanovich, S., Bene, L., Matko, J., Matyus, L., Krasznai, Z., Szabo, G., Jr., Pieri, C., Gaspar, R., Jr., & Szollosi, J. (1999) *Biophys. Chem.* **82,** 99–108.
2. Simon, R., Yang, B., Moore, S. E., Dohorty, P., Walsh, F. S. & Jacobson, K. A. (1998) *Biophys. J.* **74,** 297–308.
3. Hildebrand, C. & Waxman, S. G. (1983) *Brain Res.* **258,** 23–32.
4. Clay, J. R. & Kuzirian, A. M. (2000) *J. Neurobiol.* **45,** 172–184.
5. Clay, J. R. & Kuzirian, A. M. (1999) *Biol. Bull.* **197,** 231–232.
6. Clay, J. R. & Kuzirian, A. M. (2002) *J. Neurosci. Res.* **67,** 745–752.
7. Bray, D., Levin, M. D. & Morton-Firth, C. J. (1998) *Nature* **393,** 85–88.
8. Atri, A., Amundson, J., Clapham, D. & Sneyd, J. (1993) *Biophys. J.* **65,** 1727–1739.
9. Keizer, J. & Smith, G. D. (1998) *Biophys. Chem.* **72,** 87–100.
10. Falcke, M., Tsimring, L. & Levine, H. (2000) *Phys. Rev. E Stat. Phys. Plasmas Fluids Relat. Interdiscip. Top.* **62,** 2636–2643.
11. Walker, J. W., Somlyo, A. V., Goldman, Y. E., Somlyo, A. P. & Trentham, D. R. (1989) *Nature* **339,** 317–320.
12. Dupont, G., Swillens, S., Clair, C., Tordjman, T. & Combettes, L. (2000) *Biochim. Biophys. Acta* **1498,** 134–152.
13. Charles, A. (1998) *Glia* **24,** 39–49.
14. Klepeis, V. E., Cornell-Bell, A. H. & Trinkaus-Randall, V. (2001) *J. Cell Sci.* **114,** 4185–4195.
15. Callamaras, N., Marchant, J. S., Sun, X.-P. & Parker, I. (1998) *J. Physiol. (London)* **509,** 81–91.
16. Callamaras, N., Sun, X.-P., Ivorra, I. & Parker, I. (1998) *J. Physiol. (London)* **511,** 395–405.
17. Swillens, S., Dupont, G., Combettes, L. & Champeil, P. (1999) *Proc. Natl. Acad. Sci. USA* **96,** 13750–13755.
18. De Young, G. & Keizer, J. (1992) *Proc. Natl. Acad. Sci. USA* **89,** 9895–9899.
19. Li, Y. & Rinzel, J. (1994) *J. Theor. Biol.* **166,** 461–473.
20. Shuai, J. W. & Jung, P. (2002) *Biophys. J.* **83,** 87–97.
21. Shuai, J. W. & Jung, P. (2003) in *Function and Regulation of Cellular Systems: Experiments and Models*, eds. Deutsch, A., Howard, J., Falcke, M. & Zimmermann, W. (Springer, New York), in press.
22. Schneidman, E., Freedman, B. & Segev, I. (1998) *Neural Comput.* **10,** 1679–1703.
23. Albritton, N. L., Meyer, T. & Streyer, L. (1992) *Science* **258,** 1812–1815.
24. Shuai, J. W. & Jung, P. (2002) *Phys. Rev. Lett.* **88,** 681021–681024.
25. Schmid, G., Goychuk, I. & Hanggi, P. (2001) *Europhys. Lett.* **56,** 22–28.
26. Jung, P. & Shuai, J. W. (2001) *Europhys. Lett.* **56,** 29–35.
27. Neiman, A., Schimansky-Geier, L., Cornell-Bell, A. & Moss, F. (1999) *Phys. Rev. Lett.* **83,** 4896–4899.